ADVANCED THERAPEUTICS
www.advtherap.com

Effective Delivery of the CRISPR/Cas9 System Enabled by Functionalized Mesoporous Silica Nanoparticles for GFP-Tagged Paxillin Knock-In

Xiaoyu Xu, Oliver Koivisto, Chang Liu, Junnian Zhou, Mitro Miihkinen, Guillaume Jacquemet, Daqi Wang, Jessica M. Rosenholm, Yilai Shu,* and Hongbo Zhang**

In this study, direct and effective intracellular delivery of CRISPR/Cas9 plasmids for homology-directed repair is achieved by functionalized mesoporous silica nanoparticles (MSNs). The functionalized MSNs (Cy5.5-MSNs-NLS) are synthesized by in situ labeling of a fluorescent dye (Cy5.5) and surface conjugation of nuclear localization sequence (NLS, PKKKRKV), showing a high loading efficiency (50%) toward the plasmids (PXN cutdown plasmid: GFP-Cas9-paxillin_gRNA and repair plasmid: AICSDP-1: PXN-EGFP). Subsequently, a polymeric coating of the poly(dimethyldiallylammonium chloride) (PDDA) is electrostatically deposited onto the plasmid-loaded Cy5.5-MSNs-NLS by microfluidic nanoprecipitation. The coating layer offers effective protection against the denaturation of plasmids by EcoRV restriction enzymes, and is shown to prevent premature release. Moreover, owing to the positive charge and pH-responsive disaggregation of PDDA, enhanced cellular internalization (16 h) and endosomal escape (4 h) of the nanocarrier are observed. After escape of nanocarrier system into the cytoplasm, the NLS on the surface of MSNs facilitates nuclear transport of the CRISPR/Cas9 plasmids, achieving successful GFP-tag knock-in of the PXN genomic sequence in U2OS cells. This intracellular delivery system thus offers an attractive method to overcome physiological barriers for CRISPR/Cas9 delivery, showing considerable promise for paxillin-associated focal adhesion and signaling regulator investigation.

1. Introduction

Genome-editing technology has opened up new horizons for the treatment of a wide range of diseases, and thus might become a revolutional tool in the gene-therapy field.[1] Among different genome editing tools, Clustered Regularly Interspaced Short Palindromic Repeats (CRISPR)-associated protein 9 (Cas9) is the most promising one, which uses single guide RNA (sgRNA) for site recognition.[2,3] After cleaving by Cas9 protein, the DNA strands can be repaired by nonhomologous end-joining or homology-directed repair (HDR).[4,5] Currently, CRISPR/Cas9 technology has shown tremendous promise for biomedical research due to its versatility, simplicity, efficiency, and high specificity.[6–9]

Although CRISPR/Cas9 has shown many advantages in potential applications, the major challenge for the efficient delivery of CRISPR/Cas9 remains. Compensating for the side effects of viral vectors (high off-target effects, restricted packaging capacity, and immunogenicity),[10] some nonviral-based delivery systems, such as DNA nanoclews,[11] cationic lipids or polymers,[12,13] and gold nanoparticles,[14] have been developed for CRISPR/Cas9

Dr. X. Xu, O. Koivisto, C. Liu, Prof. J. Zhou, Prof. J. M. Rosenholm, Prof. H. Zhang
Pharmaceutical Sciences Laboratory
Åbo Akademi University
Turku 20520, Finland
E-mail: jessica.rosenholm@abo.fi; hongbo.zhang@abo.fi

The ORCID identification number(s) for the author(s) of this article can be found under https://doi.org/10.1002/adtp.202000072

DOI: 10.1002/adtp.202000072

O. Koivisto
Department of Biology
Faculty of Science and Engineering
University of Turku
Turku 20014, Finland

Prof. J. Zhou
Experimental Hematology and Biochemistry Lab
Beijing Institute of Radiation Medicine
Beijing 100850, China

M. Miihkinen, Dr. G. Jacquemet, Prof. H. Zhang
Turku Bioscience Centre
University of Turku and Åbo Akademi University
Turku 20520, Finland

Dr. G. Jacquemet
Faculty of Science and Engineering
Åbo Akademi University
Turku 20520, Finland

delivery in recent research reports. However, considering the high toxicity or high preparation costs, some of the delivery systems still challenge the effectiveness and potency of harnessing CRISPR/Cas9´s technological development. Simultaneously, for many nanocarriers with polyethyleneimine or cationic lipid modification, the CRISPR/Cas9 is conjugated or adsorbed onto the carrier surface,[15] which cannot effectively protect the CRISPR/Cas9 from denaturation while the cationic modifying materials can increase cytotoxicity to some extent. Furthermore, in most cases, unspecific delivery has shown to induce off-target effects that may result in severe side-effects.[16] Considering the above issues, devising new carriers for CRISPR/Cas9 delivery with high biocompatibility, better protectivity, and targeted editing ability are highly desirable, especially for the HDR pathway with low editing efficiency.

Among the variety of nanoparticles developed to date, mesoporous silica nanoparticles (MSNs) have emerged as an efficient delivery platform due to their high and adjustable porosity, easy surface manipulation, biocompatibility, biodegradability, and ease of preparation in large quantity with low cost.[17–19] MSNs have been used for delivering plasmid DNAs (pDNAs) for gene therapy.[20–22] However, because of the freely accessible pores of MSNs and surface adsorption loading mechanism, the carried pDNAs lack efficient protection from environmental conditions, which can result in premature pDNAs release or degradation. More recently, encapsulating the drug-loaded MSNs within a polymer matrix to seal the pores can more efficiently protect and tailor the release kinetics of the active compounds.[23–25] Moreover, the encapsulating process can be widely improved by microfluidic technology that can process and manipulate nanoliter volumes in microscale fluidic channels, leading to narrow size distribution and high batch-to-batch reproducibility.[26–28] Therefore, encapsulating the pDNA-loaded MSNs within a polymer matrix assisted by the microfluidic approach should be an ideal strategy for advanced gene editing system preparation.

In this study, we report a proof-of-concept study of using a functionalized MSNs-based nanocarrier for active and safe intracellular delivery of CRISPR/Cas9 plasmids for PXN gene knock-in trough HDR pathway. Paxillin, one of the first proteins recruited to nascent adhesions, serves as a scaffolding protein for kinases (Src, FAK), guanosine-5'-triphosphate (GTP) exchange factors, and other structural proteins, and plays a key role in assembly and disassembly of focal adhesions. It performs critical functions in coordinating the signaling events between the local tumor microenvironment and tumors cells, which can influence the tumor dissemination and metastasis.[29] Therefore, mutation in the PXN gene, as well as abnormal expression of paxillin protein, has been implicated in the progression of various cancers.[30,31] For this purpose, nuclear localization sequence (NLS)-conjugated MSNs were prepared, which could further immobilize the plasmids with high loading efficiency (50%). After pH-responsive polymer (poly(dimethyldiallylammonium chloride), PDDA) coating in water assisted by microfluidic technology, the positively charged nanocarrier can efficiently protect loaded plasmids, and subsequently it can enhance the cellular internalization and endosomal escape. Two different plasmids used for PXN gene cutdown (GFP-Cas9-paxillin_gRNA) and repair (AICSDP-1: PXN-EGFP) are then transported to the nucleus to initiate the specific GFP-tag knock-in of the PXN genomic sequence. Compared to previous nanoparticle-based methods for CRISPR/Cas9 delivery, these proof-of-concept-functionalized MSN nanocarriers can overcome different physical barriers and effectively deliver CRISPR/Cas9 plasmids into cells, enabling the successful recovery of the edited gene by HDR.

2. Results and Discussion

2.1. Preparation and Characterization of pCas9pPXN@NPs@PDDA

The design and synthetic strategy of MSNs-based nanocarrier for CRISPR/Cas9 plasmid are illustrated in **Scheme 1**. Red emitting fluorescein dye (Sulfo-Cyanine5.5 NHS ester, Cy5.5)-incorporated MSNs were achieved via a one-pot bi-phase stratification approach for intracellular visualization of the particles.[32] As shown in **Figure 1**a, the dye-loaded MSNs particles (Cy5.5-MSNs) exhibit high monodispersity and have uniform spherical morphology with an average size of 100 nm with a well-defined mesoporous structure. The hydrodynamic size of Cy5.5-MSNs in water is around 110 nm in diameter (Figure S1, Supporting Information), which is theoretically suitable for high cellular uptake and penetration into tumors due to the enhanced permeability and retention effect.[33] Successful dye incorporation can be demonstrated by UV-vis absorbance spectra (Figure S2, Supporting Information), which show an obvious absorbance band of Cy5.5 in Cy5.5-MSNs. Following surfactant extraction, the surface of Cy5.5-MSNs was modified with amine moieties via post-synthesis grafting of an aminopropylsilane for further peptide conjugation, the success of which could be verified by Fourier-transform infrared spectroscopy analysis (Figure S3, Supporting Information): $\nu_{sym}(NH_2)$: 3353 cm^{-1}, $\nu_{asym}(NH_2)$: 3268 cm^{-1}; $\delta(NH_2)$: 1636 cm^{-1}.[34] After surface modification, the uniform spherical morphology was still maintained (Figure 1b), while the zeta potential changed significantly from −15.9 to +7.0 mV due to the positively charged amino groups (Figure S4a, Supporting Information).

Later, NLS (PKKKRKV) was conjugated onto the outer surface of amine-modified Cy5.5-MSNs (Cy5.5-MSNs-NH_2), referred to as Cy5.5-MSNs-NLS, through a typical amidation process.[17] NLS is one general type of nucleus targeting signal peptide that can facilitate the transfection of DNA.[35] The NLS-modification strategy does not induce any significant difference in particle size (Figure 1c) compared with Cy5.5-MSNs, but it can play an important role for CRISPR/Cas9 plasmid delivery to the nucleus.

To improve the loading efficiency of the negatively charged CRISPR/Cas9 plasmids, the net surface charge by means of zeta potential of Cy5.5-MSNs-NLS in buffers of different pH was

Dr. D. Wang, Prof. Y. Shu
ENT Institute and Otorhinolaryngology Department of the Affiliated Eye and ENT Hospital
State Key Laboratory of Medical Neurobiology
Institutes of Biomedical Sciences
NHC Key Laboratory of Hearing Medicine
Fudan University
Shanghai 200031, China
E-mail: yilai_shu@fudan.edu.cn

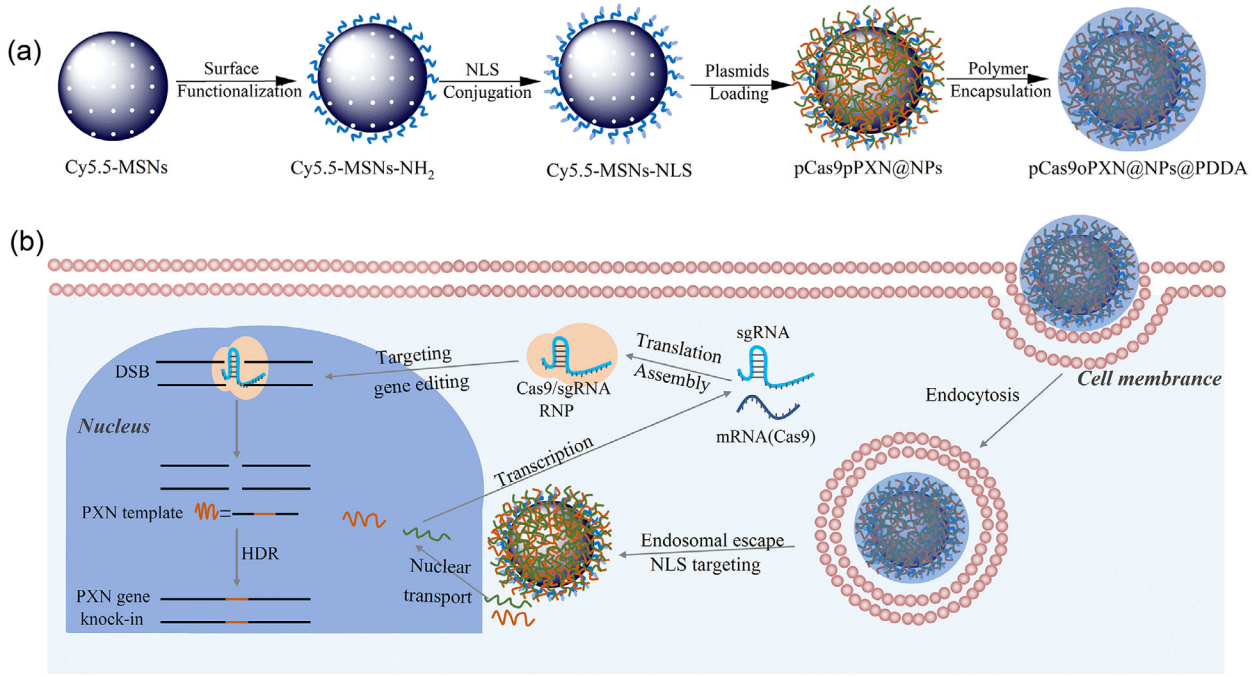

Scheme 1. Schematic illustration of the functionalized MSNs-based nanocarrier for the delivery of CRISPR/Cas9 plasmids: a) preparation of Cy5.5-MSNs-NLS, plasmid loading, and polymer encapsulation; b) intracellular delivery of the two kinds of plasmids to the nucleus for paxillin gene knock in.

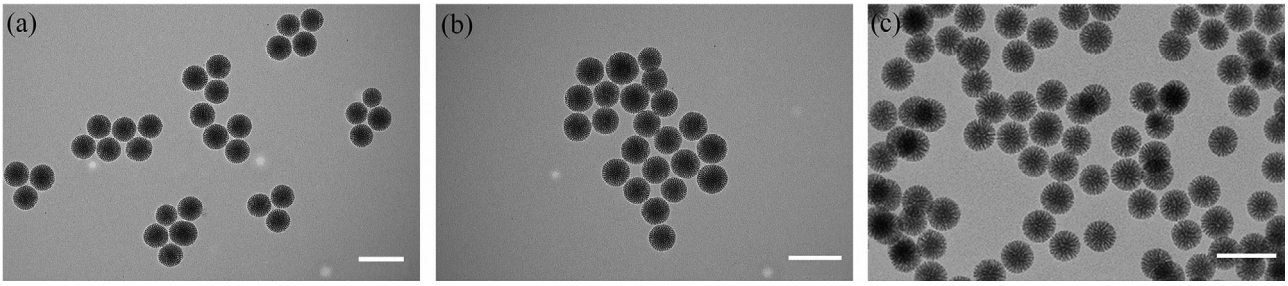

Figure 1. TEM micrographs of prepared a) Cy5.5-MSNs, b) Cy5.5-MSNs-NH_2, and c) Cy5.5-MSNs-NLS. Scale bar: 200 nm.

explored. As shown in Figure S4b in the Supporting Information, the highest positive net surface charge can be achieved in a pH 6.5 buffered solution. Thus, the synthesized Cy5.5-MSNs-NLS was mixed with both plasmids (GFP-Cas9-paxillin_gRNA (pCas9) and AICSDP-1: PXN-EGFP (pPXN)) in 4-(2-hydroxyethyl)-1-piperazineethanesulfonic acid (HEPES) buffer solution (pH = 6.5) under continuous stirring at 4 °C overnight to load the gene-editing system into the nanocarrier, which was denoted as pCas9pPXN@Cy5.5-MSNs-NLS. The molar ratio of the two plasmids was 1:1. After plasmid loading, the zeta potential of the complexes manifests a highly negative value, −23 mV (Figure S4a, Supporting Information). The loading capacity of Cy5.5-MSNs-NLS to pCas9 and pPXN was calculated to be 50 μg mg^{-1} by quantification of the plasmids via NanoDrop (2000c), indicating the synthesized Cy5.5-MSNs-NLS particles can act as nanocarriers to efficiently incorporate the CRISPR/Cas9 gene-editing plasmids.

The plasmid-loaded Cy5.5-MSNs-NLS is encapsulated within PDDA using microfluidic nanoprecipitation. The polyelectrolyte, PDDA, provides a pH-controlled molecular gate for storage and release of the plasmids from Cy5.5-MSNs-NLS. The pCas9pPXN@Cy5.5-MSNs-NLS (pCas9pPXN@NPs) and PDDA are mixed in water to form a stable system, in which PDDA adsorbed to anionic pCas9pPXN@NPs by oppositely charged ionic interaction, and then pumped into the microfluidics inner capillary. As the outer flow, absolute ethanol, rapidly diffuses to the inner flow and leads to precipitation of PDDA on top of pCas9pPXN@NPs (**Figure 2**a), referred to as pCas9pPXN@NPs@PDDA. The precipitation process is fast and after that the PDDA shell forms, which would not produce negative effect on the function of plasmids.

As described in our previous study, the coating layer thickness and encapsulation efficiency can be adjusted by changing the concentration of NPs and polymer, and the flow ratio and flow rates of the two flows in the microfluidic system.[36] In this work, we have applied the concentration ratio 1:2.5 (mg mL^{-1}) of pCas9pPXN@NPs to PDDA and the flow rates of inner and outer flow as 2:40 (mL h^{-1}), which gives the optimal conditions for

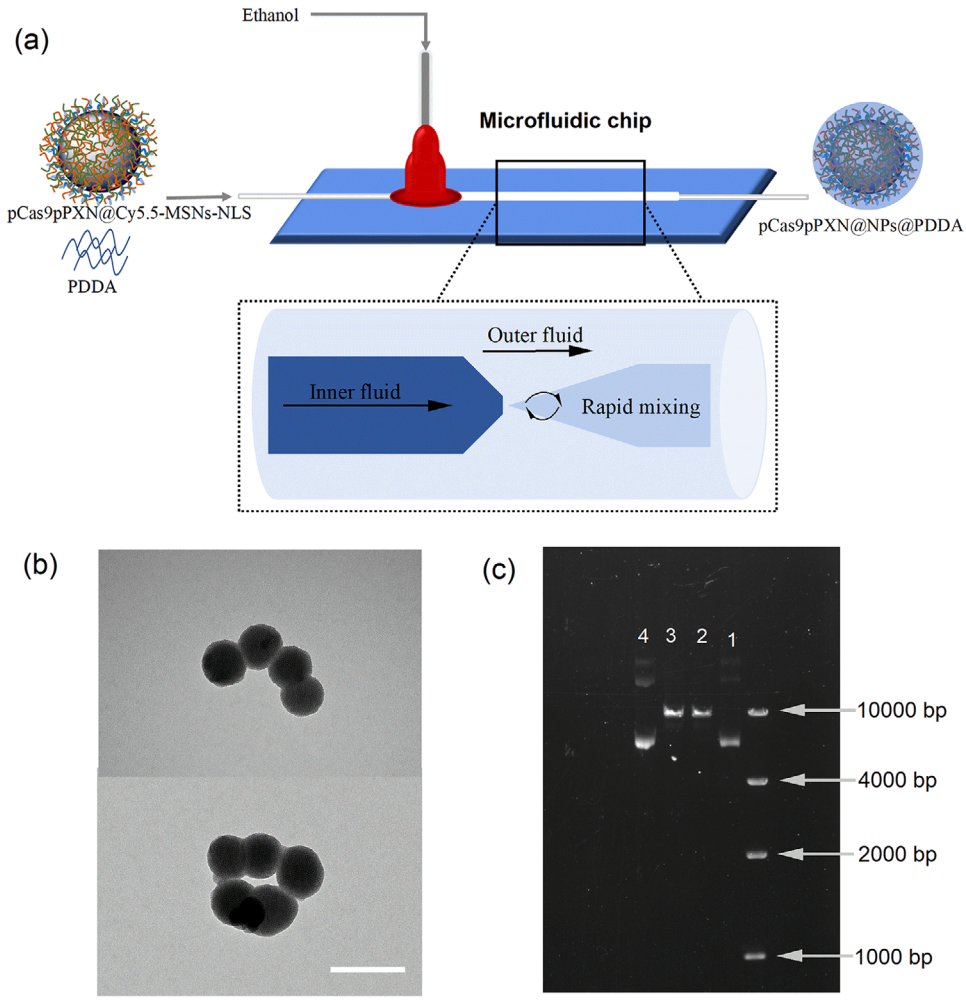

Figure 2. a) Schematics of the process to coating PDDA outside of the plasmid-loaded nanoparticles using microfluidic co-flow focusing nanoprecipitation method; b) TEM micrograph of the prepared pCas9pPXN@NPs@PDDA consisting of the polymer light gray outer region, scale bar: 200 nm; c) 0.8% agarose gel electrophoresis image of EcoRV digestion assay (100 V, 80 min) stained with the intercalating agent ethidium bromide (10 mg mL^{-1}): Lane M: DNA ladder, lane 1: naked pCas9, lane 2: EcoRV-treated pCas9, lane 3: the releasing pCas9 from pCas9@NPs after EcoRV treatment, lane 4: the releasing pCas9 from pCas9@NPs@PDDA after EcoRV treatment.

efficient encapsulation. As illustrated in Figure 2b, a clear PDDA shell can be observed outside the NPs and the pores of MSN have been fully sealed after encapsulation. Furthermore, zeta potential values shifted to +25 mV with the PDDA matrix coating (Figure S4a, Supporting Information). To facilitate the biological experiments, the particle colloidal stability was investigated by measuring the hydrodynamic size and zeta potential in cell culture media, i.e., Dulbecco's modified eagle's medium (DMEM) with 10% fetal bovine serum (FBS). The particles maintained good dispersibility after 24 h incubation in DMEM (Table S1, Supporting Information). Moreover, the PDDA shell can effectively protect the CRISPR/Cas9 plasmids against degradation by restriction enzymes. An agarose gel electrophoresis of EcoRV-digested pCas9, which has one EcoRV recognition site was performed after mixing them for 2 h at 37 °C. As shown in Figure 2c, the released pCas9 from the nanocarrier with PDDA (lane: 4) has the same ladder with the control one (lane 1), indicating that the plasmid backbone was maintained. In contrast, the released pCas9 from the nanocarrier without PDDA (lane 3) migrates slower due to the digestion to form the linearized DNA conformation.

2.2. In Vitro pH-Responsive Release of Plasmids

To evaluate the pH-responsive cargo release, the plasmid-loaded nanocarrier was immersed in phosphate-buffered saline (PBS) buffer at different pH values and the mass transport from nanocarrier to solution was detected by UV-vis spectrophotometry. **Figure 3**a shows the dependence of the released amount of plasmid over time at pH values of 7.4 and 5.5, respectively. Notably, the release rate is fast at pH 5.5, and the released amount reaches a maximum value of 33% at 35 h. Although no complete release accomplished due to the electrostatic interaction between plasmids and functionalized MSNs, the high loading efficiency could help to address this issue to achieve the editing. This pH-responsive release is mainly due to the charge reversal of loaded

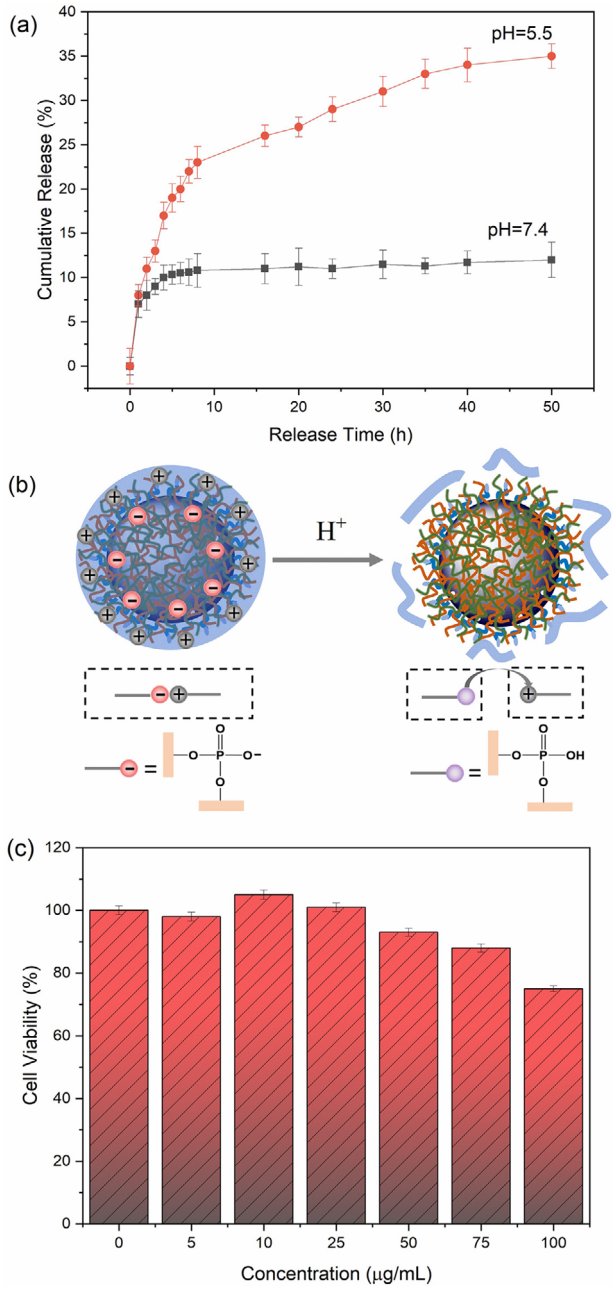

Figure 3. a) Cumulative release profile of CRISPR/Cas9 plasmids from PDDA-coated nanocarrier at different pH buffer (37 °C) as a function of incubation time measured by NanoDrop; b) schematic representation of pH-responsive plasmids release based on the interaction between negative phosphate acid species of loaded plasmids with polycations (PDDA), c) WST-1 results of U2OS cells cultured with various concentration of pCas9pPXN@NPs@PDDA (0–100 μg mL^{-1}). Bar chart represents the mean and standard deviation of three independent measurements.

plasmids, which can be transformed from ionized phosphate acid species (-$PO4^{-}$) to protonated groups (-PO_4H) by decreasing the pH value as depicted in Figure 3b. Subsequently, the electrostatic interaction between positively charged PDDA and negatively charged plasmids loaded into pCas9pPXN@NPs@PDDA is weakened with increasing acidity. Consequently, the polycations are separated from the surface of pCas9pPXN@NPs@PDDA, leading to the release of the plasmid.[37] On the contrary, at pH 7.4, the release amount is quite low and remains essentially constant (≈10%), which suggests that the state of the gates around the mesopores is still closed due to the interaction between positively charged PDDA and negatively charged plasmid. The disassembly of PDDA coating in acidic conditions can also be confirmed by transmission electron microscopy (TEM) imaging after treating the pCas9pPXN@NPs@PDDA at pH 5.5 for 10 h (Figure S5, Supporting Information).

2.3. In Vitro Cytotoxicity and Cellular Uptake

Low cytotoxicity and high biocompatibility are important features for any biomaterials. To determine the impact of pCas9pPXN@NPs@PDDA on cell viability, WST-1 assay was conducted on human bone osteosarcoma epithelial cells (U2OS) for 48 h. As shown in Figure 3c, there were no significant changes in cell viability for pCas9pPXN@NPs@PDDA at different concentrations up to 100 μg mL^{-1}, compared to that of the control group.

For effective CRISPR/Cas9-based gene editing, it is crucial for pCas9pPXN@NPs@PDDA to be efficiently internalized into the targeted cells. Based on the cytotoxicity measurement results, a concentration of 50 μg mL^{-1} of pCas9pPXN@NPs@PDDA was used for incubating with U2OS cells at different time points. The cellular uptake behavior of pCas9pPXN@NPs@PDDA (red fluorescence from Cy5.5) was evaluated with confocal laser scanning microscopy (CLSM) and flow cytometry. pCas9pPXN@NPs were also employed in this study for comparison. As shown in **Figure 4**a, the red signal from pCas9pPXN@NPs@PDDA increases gradually over time. After 16 h incubation, an obvious uptake of pCas9pPXN@NPs@PDDA is observed. In contrast, a much lower level of uptake is detected from the cells treated with pCas9pPXN@NPs. These observations were further confirmed with flow cytometry analysis (Figure 4b). The quantitative analysis results indicate that lower uptake efficiency can be obtained from the cells incubated with pCas9pPXN@NPs, whereas an enhanced uptake efficiency (1.3-fold) was occurred in the pCas9@NPs@PDDA treated cells, which can be caused by the positive PDDA layer coated on the surface of the nanocarriers.

2.4. Endosomal Escape and Nucleus-Targeting Capability

For efficient gene editing, endosomal escape is another key characteristic for the nanocarriers. It has been reported that many pH-responsive polymers can facilitate endosomal escape when degraded inside the endosome.[38,39] To investigate the endosomal escape capability, Cy5.5-labeled nanocarriers with PDDA (pCas9pPXN@NPs@PDDA) were exposed to U2OS cells, and the cells were then observed using CLSM after 1, 2, and 4 h incubation. The endosomes of the cells were stained with LysoTracker Green before confocal microscopy observation. As shown in **Figure 5**a, the colocalizations (yellow) of the nanocarriers and endosomes can be observed after 2 h incubation, indicating the entrapment of the pCas9pPXN@NPs@PDDA in endosomes. However, at 4 h, the red fluorescence signal is rather observed

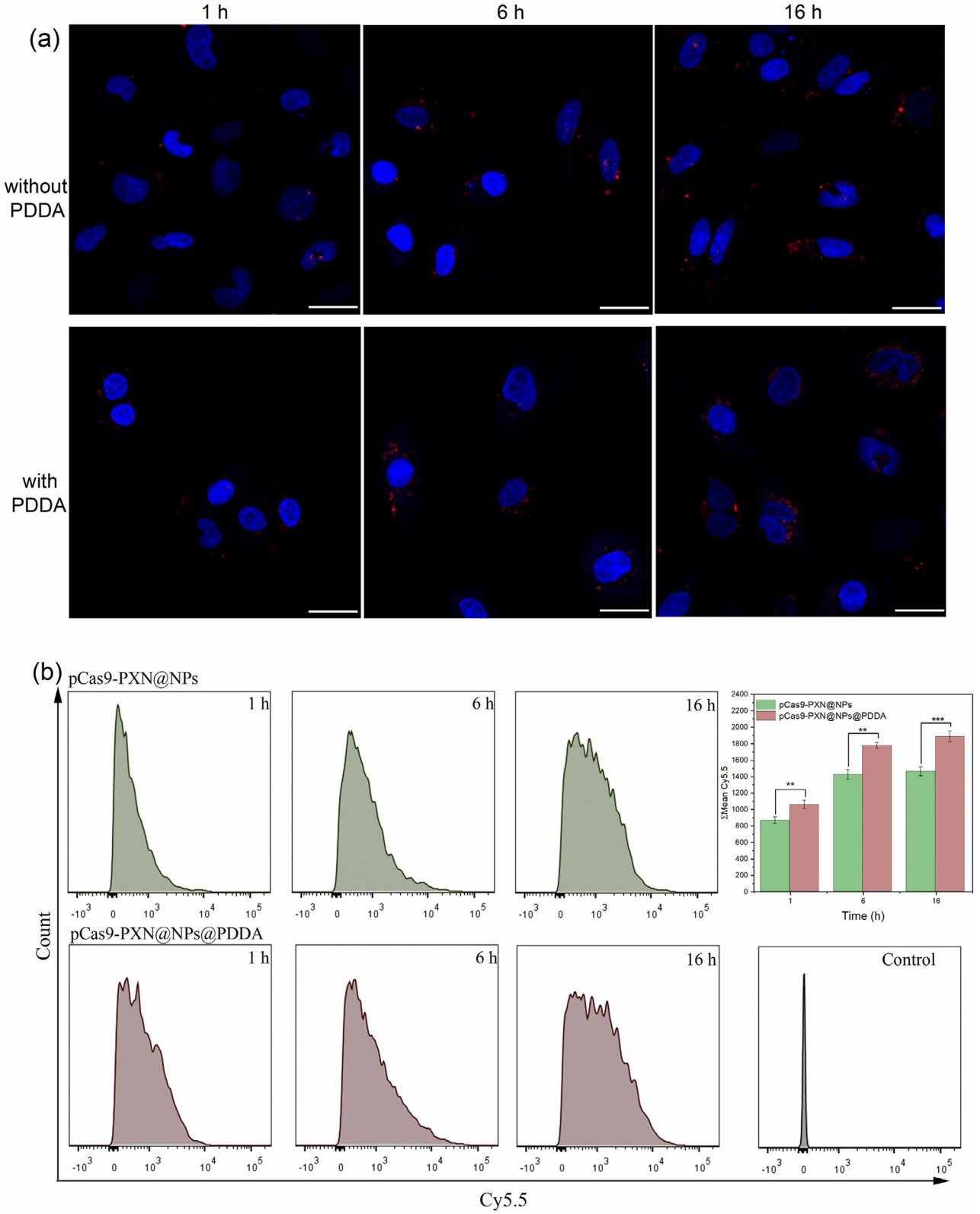

Figure 4. Cellular uptake and intracellular distribution of the plasmids-loaded nanocarriers with and without PDDA after 1, 6, and 16 h incubation detected by a) confocal microscopy and b) flow cytometry. The nanocarriers are red signal with Cy5.5, while the nuclei were stained with DAPI. The intensity of Cy5.5 was determined by the mean value in FlowJo. Two-sample *t*-test was performed, ***$p < 0.001$, **$p < 0.01$, and *$p < 0.05$. Bar chart represents the mean with standard deviations from tree independent measurements. Scale bar: 20 μm.

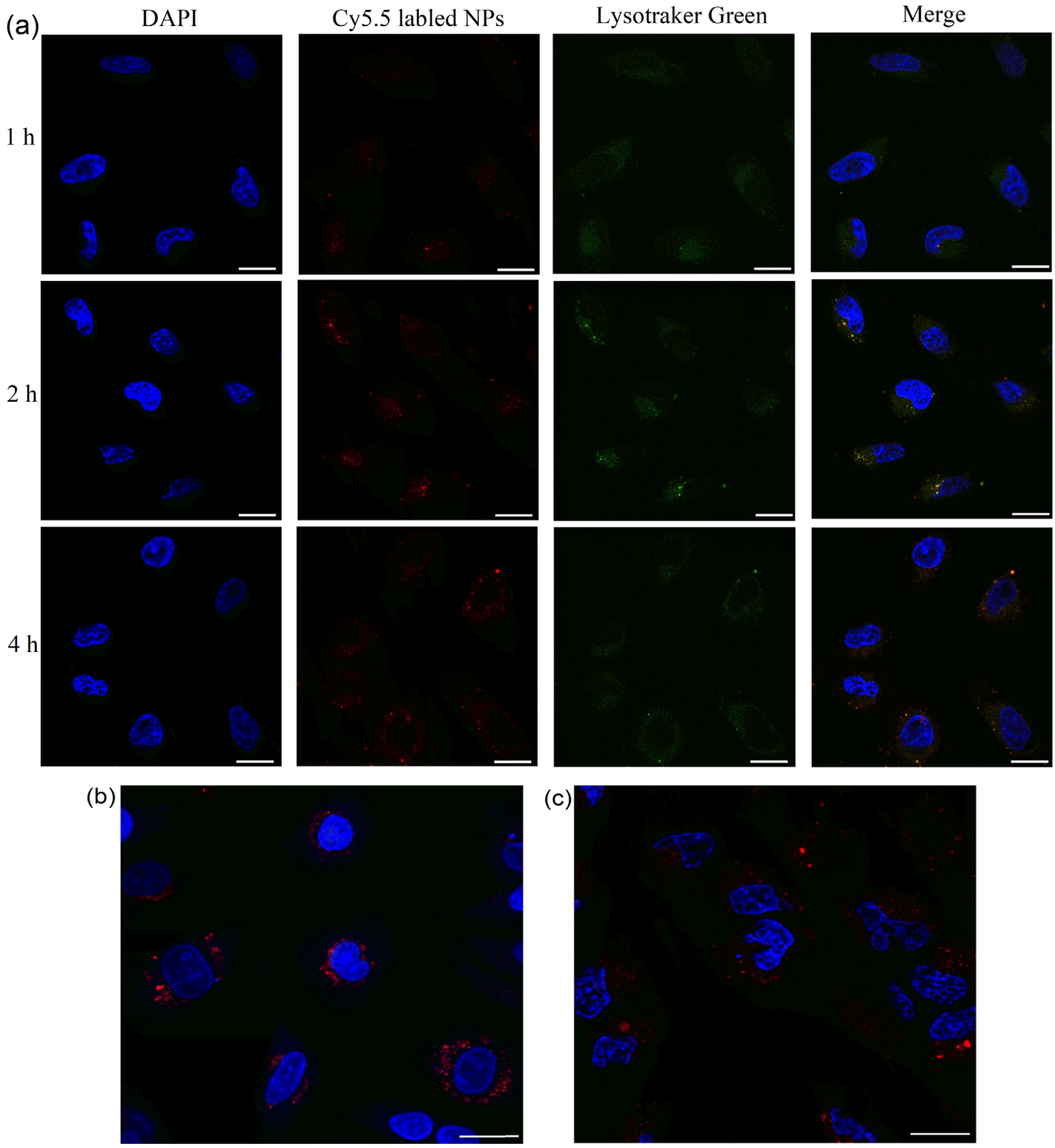

Figure 5. a) CLSM images (63 ×) of U2OS cells after incubation with pCas9pPXN@NPs@PDDA (red) for 1, 2, and 4 h. Lysotracker@Green (green) was used to stain the acidic organelles (endosomes) and DAPI was used to stain the nucleus. Co-localization was indicated by yellow fluorescence. b) Intracellular distribution of the nanocarriers b) with and c) without NLS sequence after treating the U2OS cells with 24 h. Scale bar: 20 μm.

in the nanocarrier group, implying the successful endosomal escape of the nanocarrier system. In contrast, the nanocarrier without PDDA (pCas9pPXN@NPs) shows lower endosomal escape efficiency after 4 h treatment (Figure S6, Supporting Information), indicating the key role of the pH-responsive polymer to overcome the endosomal escape abyss. Following that, the intracellular distribution of NPs is also evaluated. As presented in Figure 5b, the escaped NPs accumulate in the vicinity of the nucleus due to the presence of NLS, promoting the pCas9 and pPXN penetrating into the nucleus. In contrast, the NPs without NLS are widely distributed in the cytosol and show no obvious targeting ability to the nucleus (Figure 5c). These results demonstrate

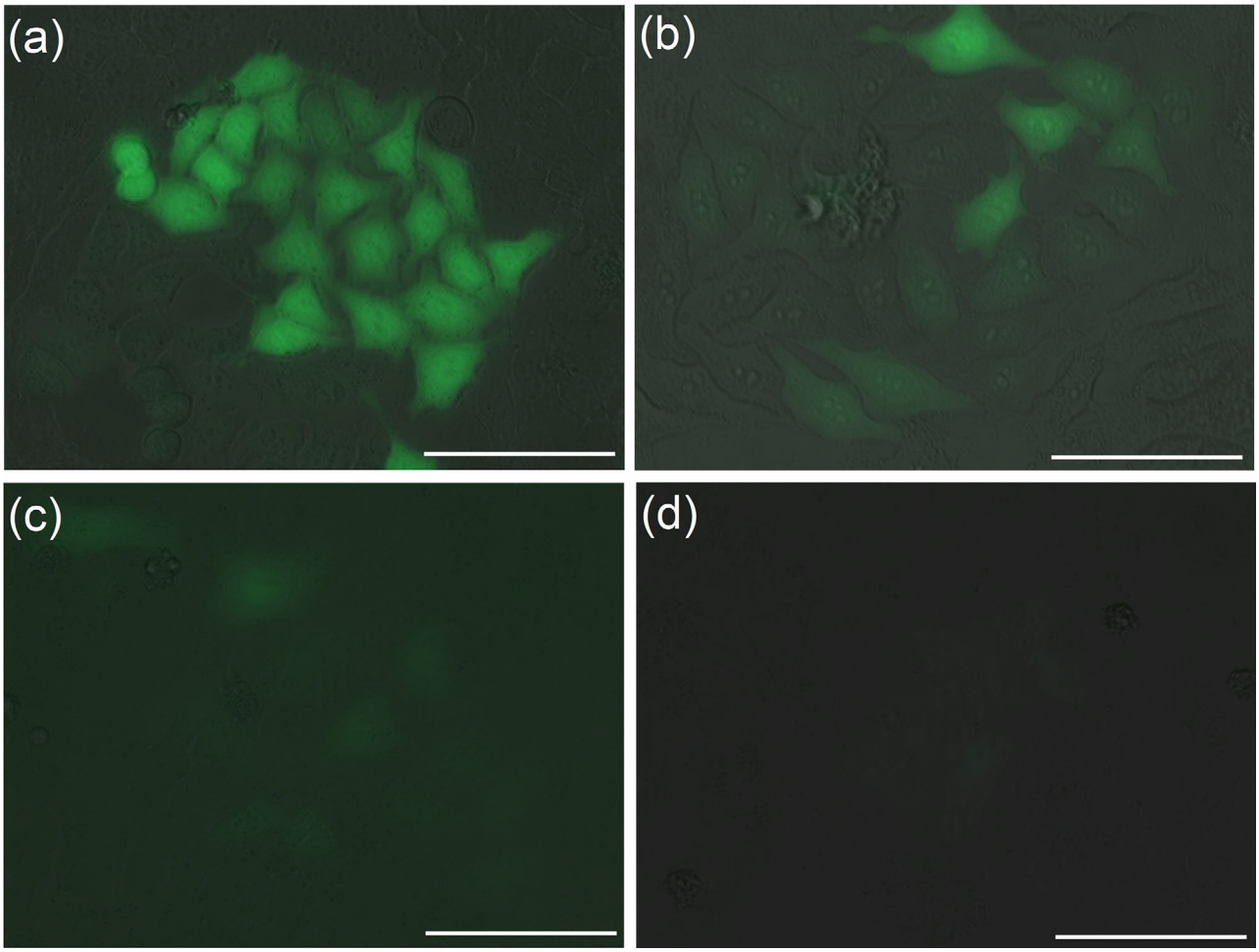

Figure 6. Fluorescence microscopy images of U2OS cells treated with pCas9@NPs@PDDA (50 μg mL^{-1}) after a) 2, b) 4, c) 6, and d) 7 days incubation to confirm the in vitro transfection and GFP expression. Scale bar: 100 μm.

that the designed nanocarrier can effectively promote the endosomal escape and deliver the pCas9 and pPXN close to the nucleus.

2.5. In Vitro Gene Expression

To further evaluate the capability of the nanocarrier for CRISPR/Cas9 plasmid delivery, we next examine the expression of the plasmids in the target cells. Here, we take pCas9 as an example. The pCas9 encoding Cas9 and sgRNA scaffold has been fused with GFP expressing sequence oligos in the downstream, which can be used as a fluorescent marker.[40] To track the green signal at different time points after transfection, we culture the U2OS cells with pCas9, NPs@PDDA, and pCas9@NPs@PDDA and observed them after 2, 4, 6, and 7 days. As shown in **Figure 6**a, the obvious GFP signal from a block proportion of U2OS cells can be observed through fluorescence microscopy after 2 days treatment with pCas9@NPs@PDDA. In contrast, no GFP signal was detected by treating U2OS cells with free pCas9 or pure NPs@PDDA (not shown), indicating the importance of using the designed delivery platform for the plasmid transfection. Nevertheless, due to the plasmid dilution with cell division, the GFP positive cell population decreases dramatically. After 4 (Figure 6b) and 6 days (Figure 6c) treatment, lower expression signal can be measured and the GFP signal almost disappears when incubating the cells for 7 days (Figure 6d).

2.6. In Vitro Gene Knock-In

To confirm the gene editing efficiency of the designed nanocarrier, we have studied the in vitro PXN knock-in potency. Paxillin is a key focal adhesion protein and signaling regulator at sites of cell extracellular matrix adhesion. In this experiment, U2OS cells were transfected with the nanocarrier loaded with pCas9 and pPXN in equimolar ratio. The plasmid pCas9 that can express the sgRNA to target the coding region of the PXN and Cas9 protein is used to create double-stranded breaks (DSBs) at PXN genome. Subsequently, the donor template pPXN is used to repair the DSBs in the HDR pathway. Thus, the correct PXN sequence can be inserted into the target site. Since the PXN sequence in plasmid pPXN has been tagged with GFP-linked expression cassette, gene editing cells can be subsequently

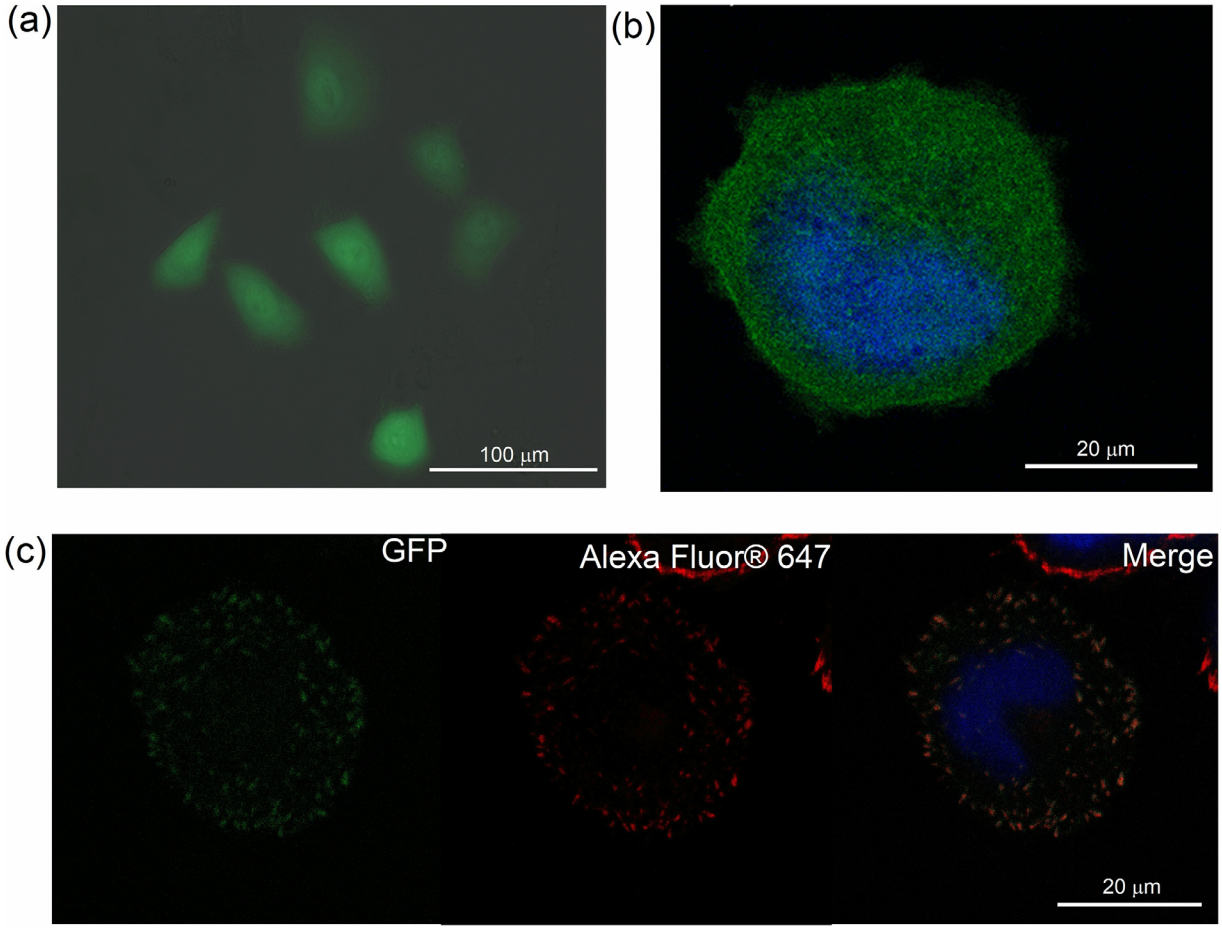

Figure 7. a) Fluorescence microscopy and b) confocal image of U2OS cells treated with pCas9pPXN@NPs@PDDA after 7 days incubation. c) Confocal immunofluorescent analysis of pCas9pPXN@NPs@PDDA-treated U2OS cells using primary antibody (anti-paxillin antibody [Y113]) and secondary antibody (anti-rabbit IgG (H+L), F(ab')2 Fragment (Alexa Fluor 647 Conjugate)) showing colocalization with GFP signals.

inspected by fluorescence microscopy. The green signal is easily distinguished from the pCas9 expression interference because of the transient expression can be disappeared after 7 days, according to the above discussion. Therefore, the gene editing behavior in U2OS cells is investigated starting from 7 days post-treatment with pCas9pPXN@NPs@PDDA. As expected, obvious GFP fluorescence can be observed by fluorescence microscopy in **Figure 7**a,b. To confirm GFP localization to the appropriated structure of paxillin, fibronectin-stained focal adhesion and immunofluorescence colocalization have been explored. Fibronectin, as the ligand for a dozen members of the integrin receptor family, could bind paxillin to achieve the transduction of environmental signals to the cell interior.[31] After plated on fibronectin, U2OS cells-localized focal adhesion sites displayed a punctate distribution with bright green fluorescence (Figure 7c). When staining the edited cells with monoclonal paxillin antibody and Alexa Fluor@647-conjugated goat anti-rabbit lgG (which was predicted to label both the GFP-tagged and untagged paxillin protein factions within the same cells), obvious colocalization of different fluorescence channels (paxillin, red and GFP, green) was observed in Figure 7c. Taken together, the results confirmed that the GFP-tagged paxillin gene has been inserted into the appropriate site of U2OS cells, which demonstrated that the functionalized MSNs-based nanocarrier was safe and specific for the CRISPR/Cas9 editing system delivery.

3. Conclusion

In summary, we have for the first time demonstrated CRISPR/Cas9 plasmid delivery by functionalized MSNs for paxillin knock-in in U2OS cells. Porous MSNs particles can effectively load large CRISPR/Cas9 plasmids with a loading efficiency of 50% and the microfluidic-based polymer (PDDA) coating can effectively protect the payloads in the nanocarrier. The electrostatic interaction between positive PDDA and the negative plasmid is weakened with increasing acidity due to the protonation of phosphate acid species (-PO^{4-}), which leads to pH responsive CRISPR/Cas9 release, and PDDA degradation induces fast endosomal escape (4 h) of the nanocarrier. By surface functionalizing the MSNs with NLS, the NPs can accumulate close to the nucleus and improve the nuclear plasmid delivery efficiency. By using GFP-Cas9-paxillin-gRNA and Cas9 plasmids as model plasmids, we have successfully knocked in the GFP-tagged paxillin into the U2OS cells genome. Therefore, this platform provides a simple but active route for the delivery

of CRISPR/Cas9 plasmids, showing considerable potential for gene editing in biomedical applications.

4. Experimental Section

Materials: Cetyltrimethylammonium chloride solution (CTAC, 25 wt% in H_2O), tetraethyl orthosilicate (TEOS, reagent grade, 98%), PDDA solution (average M_w 200 000–350 000 (medium molecular weight), 20 wt% in H_2O), paraformaldehyde (PFA, paraformaldehyde, powder, 95%), DAPI (4′,6-diamidino-2-phenylindole, for nucleic acid staining), and cell proliferation reagent (WST-1) were purchased from Sigma-Aldrich. Ammonium nitrate (NH_4NO_3, 99+%, for analysis), triethylamine (TEA, 99%, pure), and 3-aminopropyltriethoxysilane (APTES, 99%, AcroSeal) were purchased from ACROS Organics. 1-Ethyl-3-(3-dimethylaminopropyl)carbodiimide hydrochloride (EDC·HCl, > 98.0%) was purchased from Tokyo Chemical Industry Co., Ltd. (TCI)) and *N*-hydroxysuccinimide (NHS, 98+%) was purchased from Alfa Aesar. The NLS (PKKKRKV) was bought from Genscript biotech corporation (Nanjing, China). The plasmid (pCas9) that encoded with the gRNA sequence targeting paxillin (5′-GCACCTAGCAGAAGAGCTTG-3′) into pSpCas9(BB)-2A-GFP backbone, the template plasmid (AICSDP-1:PXN-EGFP, pPXN), and primary antibodies against paxillin (anti-paxillin antibody [Y113]) were kind gifts from Prof. Johanna Ivaska at Turku Bioscience Centre (Biocity, Finland). The secondary antibodies anti-rabbit IgG (H+L) conjugated to Alexa Fluor 647 were bought from Invitrogen.

Preparation of Cy5.5-Loaded MSN (Cy5.5-MSNs): The preparation of Cy5.5-MSNs was operated through a modified method by Zhao's group.[32] It was achieved via a one-pot bi-phase stratification approach by continuous growth using cationic surfactant CTAC as a template, TEOS as a silica source, TEA as a catalyst, and organic solvent cyclohexene as an emulsion agent. A typical synthesis process was performed as follows. Briefly, 24 mL (25 wt%) CTAC solution and 0.18 g of TEA were added to 36 mL water and stirred for 1 h at 60 °C. Then added 20 mL of TEOS (10 v/v%) in cyclohexene to the CTAC and TEA water solution carefully under stirring. The reaction was kept at 60 °C with gentle magnetic stirring (≈150 rpm) overnight to obtain the products. After that, the products were collected by centrifugation and washed several times with ethanol to remove the residual reactants. To remove the template, the collected products were extracted with a 0.6 wt% NH_4NO_3 ethanol solution at 60 °C for 6 h twice.

Surface Functionalization of Cy5.5-MSNs: The amine-functionalized Cy5.5-MSNs particles (Cy5.5-MSNs-NH_2) were synthesized by refluxing 50 mg of Cy5.5-MSNs and 50 µL of APTES in ethanol at 60 °C overnight (150 rpm). After 16 h, the obtained particles (Cy5.5-MSNs-NH_2) were collected with centrifugation and washed twice with ethanol.

NLS Conjugation: 2 mg (2 µmol) of NLS was dissolved in 10 mL of PBS (pH = 6) with gentle mixing. After this, 0.1 mmol of EDC (19.17 mg) and 0.15 mmol of NHS (17.26 mg) were added to the PBS solution. This mixture was then kept at stirring for 30 min to activate the carboxyl group. 20 mg of Cy5.5-MSNs-NH_2 particles were centrifuged, washed two times with PBS to get rid of the ethanol, and then added to the NLS mixture. This solution was kept at stirring for 2 h. NLS-modified MSN particles (Cy5.5-MSNs-NLS) were obtained after washing with PBS twice.

Loading of Plasmids: A stock of Cy5.5-MSNs-NLS particles (1 mg mL^{-1}) was dispersed in PBS (pH 6.0). Plasmid stock (pCas9 and pPXN mixed with 1:1 ratio) was also prepared in PBS buffer (100 µg mL^{-1}). 500 µL of plasmid stock and 500 µL of Cy5.5-MSNs-NLS stock were mixed. This mixture was kept overnight at +4 °C and under magnetic stirring in 2 mL Eppendorf tube. After overnight incubation, 100 µL of the solution was taken away to measure how much plasmids were loaded to the particles. The solution was centrifuged for 10 min at 13 400 rpm with Eppendorf MiniSpin. Plasmids that were not loaded into the particles were found in the supernatant, and were collected into a new tube. These non-loaded plasmids were collected and then assayed by using a UV-vis spectrophotometer (NanoDrop 2000c, ThermoFisher) at wavelengths of 260 and 280 nm. From the DNA concentration, both loading efficiency (LE%) and the loading capacity (LC, mg g^{-1}) were determined by using the formula below

$$\mathrm{LE}\% = \frac{A_i - A_f}{A_i} \times 100 \quad (1)$$

$$\mathrm{LC}\ (\mu g\ mg^{-1}) = \frac{A_i - A_f}{\text{amount of MSNs}} \quad (2)$$

where A_i stands for the initial and A_f for the final amount of plasmid.

Polymer Coating with Microfluidic Technology: A 3D microfluidic co-flow focusing device was fabricated by assembling two (inner and outer) glass capillaries on a glass slide. After mixing the polymer (PDDA, 1.25 mg mL^{-1}) and plasmid-loaded Cy5.5-MSN-NLS (pCas9pPXN@NPs 250 µg mL^{-1}) in water, the solution was served as inner phase, meanwhile, the pure ethanol was selected as the outer phase. The two liquids were injected separately into the microfluidic device at a constant flow rate. The flow rate of inner and outer liquids was set to 2 and 40 mL h^{-1}, which was controlled by pumps (PHD 2000, Harvard Apparatus, USA). And the coating process was monitored by using the Meros high-speed digital microscope (Dolomit microfluidics), in which the inner fluid was focused by the outer continuous fluid. In this procedure, the hydrophilic polymer would precipitate outside of the nanocarrier after meeting with ethanol to form a uniform coating layer. The coated nanocarrier (pCas9pPXN@NPs@PDDA) was obtained after centrifuging.

Characterization of the NPs: The morphology of the synthetic NPs was evaluated by a TEM (JEOL 1400 Plus, USA). Particle sizing was performed using dynamic light scattering with a Zetasizer Nano ZS (Malvern Instruments Ltd., UK). The nanocarrier surface zeta potential was measured with a Zetasizer Nano ZS by using disposable folded capillary cells (DTS1070, Malvern, UK).

In Vitro Plasmid Releasing: The in vitro release of encapsulated plasmid from PDDA-coated nanocarriers and the effect of pH on the release profiles were determined by suspending the pCas9pPXN@NPs@PDDA in 100 µL HEPES buffer with different pH (7.4 and 5.5) value at a final nanocarrier concentration of 0.5 mg mL^{-1}. All suspensions were placed in a shaker (Grant GLS400). The amount of released plasmid was determined by removing the supernatant after centrifugation (13 000 rpm, 5 min) and replacing it with a new buffer (100 µL) at the collecting time points. Then the release profile was measured using NanoDrop 2000c Fluorospectrometer (ThermoFisher, USA) and all the measurements were performed in triplicate.

EcoRV Digestion and DNA Electrophoresis Assay: *For digestion reaction*: The nuclease-free water (16 µL) and 10 × buffer R (2 µL) were mixing together and then adding 1 µL (1 µg $µL^{-1}$) pure pCas9, released pCas9 from pCas9@NPs, and released pCas9 from pCas9@NPs@PDDA separately, following by adding EcoRV (2 µL). The solution for pCas9 without EcoRV was taken as control group. Every solution was mixed gently and spun down for a few seconds. Afterward, they were incubated overnight at 37 °C water bath. *For DNA electrophoresis assay*: 8 mg of agarose powder was added to 100 mL TBE (Tris-borate-ethylenediaminetetraacetic acid, 0.5%) in a microwavable flask and microwaved for several minutes until the agarose was completely dissolved. After the agarose solution cooled down, 40 mL was taken and one drop of ethidium bromide was added to a final concentration of ≈0.2–0.5 µg mL^{-1}. Then the agarose was poured into a gel tray with the well comb and waited for 20–30 min until it had completely solidified. After that, the samples (2 µL) mixed with 6 × loading buffer (4 µL) were loaded into comb wells carefully. The FastRuler High Range DNA ladder was loaded into the first lane of the gel. The gel was placed into the gel box and run it at 100 V until the dye line was ≈75–80% of the way down the gel. Finally, the gel was imaged by ChemiDoc imager to visualize the DNA fragments.

Cell Viability Assay: The used cell line, U2OS, was a generous gift from Prof. Johanna Ivaska at Turku Bioscience Centre (Biocity, Finland). The cells were cultured in a 37 °C incubator under 5% CO_2 and 90% humidity with complete growth medium: DMEM supplemented with 10%, v/v heat-inactivated FBS, 0.5% penicillin/streptomycin solution, 1% nonessential amino acid, and 1% L-glutamine. To study cytotoxicity, WST-1 assay was

performed according to the manufacture's protocol. U2OS cells were seeded into 96-well plates (2×10^4 cells per well) one day before. Then, the cell growth medium was replaced with a fresh medium containing different concentrations of NPs@PDDA, which positive control was 100 uL DMEM with 10% dimethyl sulfoxide. After 48 h incubation, the WST-1 reagent was added to each well and the cells were incubated for 2 h at 37 °C with 5% CO_2. The absorbance was measured by a Varioskan Flash Multimode Reader (Thermo Scientific Inc., Waltham, MA, USA) at 440 nm. Triplicates were used for the experiment and averaged absorbance readings were plotted.

Cell Uptake Study: The U2OS cells were seeded and incubated overnight in confocal dishes (20×10^4 cells per dish) and 6-well plates (2×10^5 cells per well). Then the medium was replaced with the fresh medium containing pCas9pPXN@NPs@PDDA and pCas9pPXN@NPs (50 μg mL^{-1}) and incubated for another 1, 6, and 16 h at 37 °C. For CLSM (Zeiss, LSM780, Germany), the cells in confocal dishes were rinsed with PBS twice, fixed with 4% PFA, and stained with DAPI (5 μg mL^{-1}). Detection of DAPI was performed with 405 nm laser excitation and laser 633 was utilized for Cy5.5 exciting. For quantitative analysis, the cells in the 6-well plate were collected by trypsin and dispersed in PBS. Then the acquisition of cellular uptake was determined by flow cytometer BD LSRFortessa by using the Alexa Fluor 700 channel. All measurements were carried out in triplicate.

Endosome Escape and Nucleus Targeting: The U2OS cells were seeded in confocal dishes (2×10^5 cells per dish) and incubated overnight for attachment. The plasmids-loaded nanocarrier (pCas9pPXN@NPs@PDDA) was dispersed into DMEM and added to each dish (50 μg mL^{-1}, 2 mL). LysoTracker@Green probe was used to stain endosomes according to the manufacture protocol. At the determined time point (1, 2, 4 h), the cells were fixed with 4% PFA and further stained with DAPI. Then the endosomal escape and nucleus targeting ability of the nanocarrier were measured with CLSM.

In Vitro Gene Transfection Study: The U2OS cells were seeded into 24-well plate (5×10^4 cells per well) and cultured overnight. The pCas9@NPs@PDDA (1 μg NPs loaded with 500 ng plasmids) were dispersed into 1 mL DMEM culture medium and added to corresponding wells, in which the pCas9 and NPs@PDDA were used as control. After incubating for the determined time at 37 °C, the cells were analyzed by EVOS fluorescence microscopy (AMG) using a GFP filter.

Analysis of Gene Editing Efficiency: *Fibronectin staining*: Fibronectin was prepared in PBS (10 μg mL^{-1}) and confocal microscope slide was incubated into the fibronection solution at 4 °C. After overnight treatment, the glass with fibronectin was rinsed a few times with PBS. Then the transfected U2OS cells were seeded on top of the fibronectin-coated glass and incubated at room temperature for 2 h. After that, the cells were fixed with 4% PFA for 15 min at room temperature and washed with PBS three times. DAPI solution (5 μg mL^{-1}) was then added into the cells for 5 min. Then it was washed three times with PBS. *Immunofluorescence test*: After fibronectin staining, the treated cells were kept in PBS solution with 1 M glycine and then washed with PBS. To remove the cellular membrane lipid, the cells were permeabilized with 0.3% Triton X-100 in PBS (600 μL) for 2 min at room temperature. After that, cells were washed and incubated with primary antibodies 1:100 diluted in 1% bovine serum albumin (BSA) in PBS at +4 °C overnight. The samples were then washed twice with PBS and incubated with secondary antibodies diluted in 1% BSA in PBS for 1 h at room temperature. For confocal measurement, the prepared samples were washed three times with PBS.

Statistical Analysis: All results were presented as mean ± standard deviations (SD) and performed using two-sample *t*-test. The statistical significance between groups was indicated by $***p < 0.001$, $**p < 0.01$, and $*p < 0.05$, respectively.

Supporting Information

Supporting Information is available from the Wiley Online Library or from the author.

Acknowledgements

X.X. and O.K. contributed equally to this work. Authors are thankful to Prof. Johanna Ivaska for donating the U2OS cell line and plasmids used in this manuscript. Prof. Tiina Henttinen is kindly acknowledged for the helping immunofluorescence study . This work was supported by Academy of Finland (grants nos. 328933, 309373), Sigrid Jusélius Foundation, National Natural Science Foundation of China (81822011), Science and Technology Commission of Shanghai Municipality (18410712400), Åbo Akademi University Research Foundation (CoE CellMech), University of Turku foundation, and Maud Kuistila foundation.

Conflict of Interest

The authors declare no conflict of interest.

Keywords

CRISPR/Cas9 gene editing, functionalized MSNs, GFP-tagged paxillin knock-in, microfluidic technology, stimuli responsive

Received: April 13, 2020
Revised: May 28, 2020
Published online: June 15, 2020

[1] A. S. Timin, A. R. Muslimov, K. V. Lepik, O. S. Epifanovskaya, A. I. Shakirova, U. Mock, K. Riecken, M. V. Okilova, V. S. Sergeev, B. V. Afanasyev, B. Fehse, G. B. Sukhorukov, *Nanomed.: Nanotechnol., Biol. Med.* **2018**, *14*, 97.
[2] S. K. Alsaiari, S. Patil, M. Alyami, K. O. Alamoudi, F. A. Aleisa, J. S. Merzaban, M. Li, N. M. Khashab, *J. Am. Chem. Soc.* **2018**, *140*, 143.
[3] L. Cong, F. A. Ran, D. Cox, S. Lin, R. Barretto, N. Habib, P. D. Hsu, X. Wu, W. Jiang, L. A. Marraffini, F. Zhang, *Science* **2013**, *339*, 819.
[4] C. Liu, L. Zhang, H. Liu, K. Cheng, *J. Controlled Release* **2017**, *266*, 17.
[5] H. X. Wang, M. Li, C. M. Lee, S. Chakraborty, H. W. Kim, G. Bao, K. W. Leong, *Chem. Rev.* **2017**, *117*, 9874.
[6] L. Li, L. Song, X. Liu, X. Yang, X. Li, T. He, N. Wang, S. Yang, C. Yu, T. Yin, Y. Wen, Z. He, X. Wei, W. Su, Q. Wu, S. Yao, C. Gong, Y. Wei, *ACS Nano* **2017**, *11*, 95.
[7] C. Z. Long, J. R. McAnally, J. M. Shelton, A. A. Mireault, R. Bassel-Duby, E. N. Olson, *Science* **2014**, *345*, 1184.
[8] D. Heck, M. S. Kowalczyk, D. Yudovich, R. Belizaire, R. V. Puram, M. E. McConkey, A. Thielke, J. C. Aster, A. Regev, B. L. Ebert, *Nat. Biotechnol.* **2014**, *32*, 941.
[9] Y. Y. Niu, B. Shen, Y. Q. Cui, Y. C. Chen, J. Y. Wang, L. Wang, Y. Kang, X. Y. Zhao, W. Si, W. Li, A. P. Xiang, J. K. Zhou, X. J. Guo, Y. Bi, C. Y. Si, B. Hu, G. Y. Dong, H. Wang, Z. M. Zhou, T. Q. Li, T. Tan, X. Q. Pu, F. Wang, S. H. Ji, Q. Zhou, X. X. Huang, W. Z. Ji, J. H. Sha, *Cell* **2014**, *156*, 836.
[10] F. Chen, M. Alphonse, Q. Liu, *Wiley Interdiscip. Rev.: Nanomed. Nanobiotechnol.* **2020**, *12*, e1609.
[11] W. J. Sun, W. Y. Ji, J. M. Hall, Q. Y. Hu, C. Wang, C. L. Beisel, Z. Gu, *Angew. Chem., Int. Ed.* **2015**, *54*, 12029.
[12] J. A. Zuris, D. B. Thompson, Y. Shu, J. P. Guilinger, J. L. Bessen, J. H. Hu, M. L. Maeder, J. K. Joung, Z. Y. Chen, D. R. Liu, *Nat. Biotechnol.* **2015**, *33*, 73.
[13] J. Liu, J. Chang, Y. Jiang, X. D. Meng, T. M. Sun, L. Q. Mao, Q. B. Xu, M. Wang, *Adv. Mater.* **2019**, *31*, e1902575.
[14] R. Mout, M. Ray, G. Y. Tonga, Y. W. Lee, T. Tay, K. Sasaki, V. M. Rotello, *ACS Nano* **2017**, *11*, 2452.

[15] M. H. Kim, H. K. Na, Y. K. Kim, S. R. Ryoo, H. S. Cho, K. E. Lee, H. Jeon, R. Ryoo, D. H. Min, *ACS Nano* **2011**, *5*, 3568.
[16] L. Li, Z. Yang, S. J. Zhu, L. C. He, W. P. Fan, W. Tang, J. H. Zou, Z. Y. Shen, M. R. Zhang, L. G. Tang, Y. L. Dai, G. Niu, S. Hu, X. Y. Chen, *Adv. Mater.* **2019**, *31*, e1901187.
[17] M. H. Yao, M. Ma, H. B. Zhang, Y. Z. Zhang, G. Wan, J. Shen, H. R. Chen, R. Wu, *Adv. Funct. Mater.* **2018**, *28*, 1804497.
[18] A. Watermann, J. Brieger, *Nanomaterials* **2017**, *7*, 189.
[19] R. K. Kankala, H. B. Zhang, C. G. Liu, K. R. Kanubaddi, C. H. Lee, S. B. Wang, W. G. Cui, H. A. Santos, K. L. Lin, A. Z. Chen, *Adv. Funct. Mater.* **2019**, *29*, 1902652.
[20] H. Yang, K. Zheng, Z. M. Zhang, W. Shi, S. B. Jing, L. Wang, W. Zheng, D. Z. Zhao, J. N. Xu, P. Zhang, *J. Colloid Interface Sci.* **2012**, *369*, 317.
[21] E. Keles, Y. Song, D. Du, W. J. Dong, Y. H. Lin, *Biomater. Sci.* **2016**, *4*, 1291.
[22] J. Yan, X. L. Lu, X. C. Zhu, X. K. Hu, L. L. Wang, J. Qian, F. M. Zhang, M. Liu, *Int. J. Nanomed.* **2020**, *15*, 497.
[23] D. F. Liu, H. B. Zhang, E. Makila, J. Fan, B. Herranz-Blanco, C. F. Wang, R. Rosa, A. J. Ribeiro, J. Salonen, J. Hirvonen, H. A. Santos, *Biomaterials* **2015**, *39*, 249.
[24] B. G. Trewyn, I. I. Slowing, S. Giri, H. T. Chen, V. S. Y. Lin, *Acc. Chem. Res.* **2007**, *40*, 846.
[25] J. Wen, K. Yang, Y. Q. Xu, H. J. Li, F. Y. Liu, S. G. Sun, *Sci. Rep.* **2016**, *6*, 38931.
[26] G. M. Whitesides, *Nature* **2006**, *442*, 368.
[27] H. B. Zhang, W. G. Cui, X. M. Qu, H. Y. Wu, L. L. Qu, X. Zhang, E. Makila, J. Salonen, Y. Q. Zhu, Z. Yang, D. Chen, H. A. Santos, M. T. Hai, D. A. Weitz, *Proc. Natl. Acad. Sci. USA* **2019**, *116*, 7744.
[28] X. D. Ma, E. Ozliseli, Y. Z. Zhang, G. Q. Pan, D. Q. Wang, H. B. Zhang, *Biomater. Sci.* **2019**, *7*, 634.
[29] N. O. Deakin, J. Pignatelli, C. E. Turner, *Genes Cancer* **2012**, *3*, 362.
[30] C. E. Turner, *Nat. Cell Biol.* **2000**, *2*, E231.
[31] M. R. Bai, J. Xie, X. Y. Liu, X. Chen, W. J. Liu, F. Z. Wu, D. Chen, Y. M. Sun, X. Li, C. L. Wang, L. Ye, *ACS Appl. Mater. Interfaces* **2018**, *10*, 26917.
[32] D. K. Shen, J. P. Yang, X. M. Li, L. Zhou, R. Y. Zhang, W. Li, L. Chen, R. Wang, F. Zhang, D. Y. Zhao, *Nano Lett.* **2014**, *14*, 923.
[33] W. Cheng, J. P. Nie, L. Xu, C. Y. Liang, Y. Peng, G. Liu, T. Wang, L. Mei, L. Q. Huang, X. W. Zeng, *ACS Appl. Mater. Interfaces* **2017**, *9*, 18462.
[34] X. Y. Xu, X. Lian, J. N. Hao, C. Zhang, B. Yan, *Adv. Mater.* **2017**, *29*, 1702298.
[35] M. Zhao, J. Li, H. R. Ji, D. W. Chen, H. Y. Hu, *Int. J. Nanomed.* **2019**, *14*, 6519.
[36] H. B. Zhang, D. F. Liu, L. Wang, Z. H. Liu, R. R. Wu, A. Janoniene, M. Ma, G. Q. Pan, L. Baranauskiene, L. L. Zhang, W. G. Cui, V. Petrikaite, D. Matulis, H. X. Zhao, J. M. Pan, H. A. Santos, *Adv. Healthcare Mater.* **2017**, *6*, 1601406.
[37] Q. Yang, S. H. Wang, P. W. Fan, L. F. Wang, Y. Di, K. F. Lin, F. S. Xiao, *Chem. Mater.* **2005**, *17*, 5999.
[38] X. D. Xu, J. Wu, Y. L. Liu, M. Y. Yu, L. L. Zhao, X. Zhu, S. Bhasin, Q. Li, E. Ha, J. J. Shi, O. C. Farokhzad, *Angew. Chem., Int. Ed.* **2016**, *55*, 7091.
[39] S. Wannasarit, S. Q. Wang, P. Figueiredo, C. Trujillo, F. Eburnea, L. Simon-Gracia, A. Correia, Y. P. Ding, T. Teesalu, D. F. Liu, R. Wiwattanapatapee, H. A. Santos, W. Li, *Adv. Funct. Mater.* **2019**, *29*, 1905352.
[40] F. A. Ran, P. D. Hsu, J. Wright, V. Agarwala, D. A. Scott, F. Zhang, *Nat. Protoc.* **2013**, *8*, 2281.